Hybrid Delay-Phase Precoding in Wideband UM-MIMO Systems under True Time Delay and Phase Shifter Hardware Limitations

Akram Najjar, Mohammed El-Absi, and Thomas Kaiser
Institute of Digital Signal Processing, Duisburg-Essen University, Duisburg, Germany

Abstract

The exploitation of the substantial bandwidths available in the terahertz (THz) band has recently attracted considerable interest. However, beam squint effect is a significant obstacle in the design of wideband hybrid beamformers. The beam squint effect causes the radiation beam to deviate from the desired direction, resulting in substantial gain losses and hindering the effective utilization of available bandwidths. Delay-phase precoding (DPP), a combination of true time delay (TTD) elements and phase shifters (PSs) in the analog domain, has emerged as a potential solution to overcome the beam squint effect and maintain practical system design. However, existing hybrid precoding schemes that assume infinite resolution and unbounded range TTDs, as well as infinite resolution PSs, impose a significant burden in terms of hardware complexity and power consumption. In this paper, we propose the delta-delay-phase precoding (DDPP) architecture to alleviate the maximum delay range constraint of TTDs significantly, surpassing the state-of-the-art solutions in the literature. Additionally, we propose hardware-aware designs for the hybrid analog precoder to combat beam squint effect while complying with the hardware limitations of TTDs and PSs. We formulate the design of TTDs and PSs as a joint optimization problem subject to their finite-resolution constraints. To tackle this non-convex optimization problem, we propose an iterative precoding algorithm based on alternating minimization. Simulation results demonstrate the superiority of the proposed hybrid analog precoding schemes over recent literature works. Particularly, the proposed precoding schemes achieve near-optimal performance despite the hardware limitations of TTDs and PSs.

Index Terms

THz, UM-MIMO, TTD, Hybrid Precoding, Finite-resolution, Limited-range, Alternating minimization.

I. Introduction

Terahertz (THz) band, ranging between 0.1-10 THz, possesses enormous vacant bandwidths that could fulfill the demands of future bandwidth-hungry applications, such as virtual reality and holography [2]–[7]. several challenges must be addressed before reaping the benefits of this spectrum range. The spreading loss, which is proportional to the square of the carrier frequency, is a significant obstacle that hinders the utilization of THz frequencies. Additionally, molecular absorption causes attenuation that further increases the path loss in the THz band [8]. As a result, numerous efforts have been dedicated to overcome the significant losses associated with THz frequencies and extending the communication range [9]–[12].

As a result, ultra-massive multiple input multiple output (UM-MIMO) technology has become a primer focus of research activities as a key-enabler for THz communications. Due to the submillimeter-level wavelengths of signals in the THz band, the size of antenna elements is proportional to the wavelength, allowing for several thousands of antenna elements to be packed into a relatively small area [13]. This results in high gains from constructive interference between signals radiated from individual antenna elements, known as beamforming gain [14].

Beamforming can be achieved through different methods, including digital, analog, and hybrid beamforming. However, digital beamforming with a dedicated RF chain per antenna element is not practical due to the high power consumption of the huge number of RF chains and their associated digital to analog converters (DACs) [15]. Analog beamforming, on the other hand, utilizes a single RF chain but lacks the potential to multiplex different data streams, which has led to the emergence of hybrid beamforming as a compromise solution with a few number of RF chains [16], [17]. Conventional hybrid beamformers use a phase shifter (PS) network to adjust the phases of signals before radiation, with the weights of PSs typically designed for the carrier frequency and applied to the entire bandwidth. In narrowband communication systems, this approach has a negligible effect due to the convergence of frequencies. However, in wideband communication systems, the beam squint effect causes the radiation angle to vary at each frequency within the bandwidth, leading to a frequency-dependent radiation angle [18]. This becomes more severe with UM-MIMO systems, where the radiated beams are very sharp and even a slight squint can have a significant impact [19]. Therefore, frequency-dependent phase shifts are required to achieve a frequency-independent radiation angle, which is what a true time

Part of this work was accepted for publication at IEEE ICC 2023 [1].

delay (TTD) element can provide [20].

TTD elements have been proposed by several studies in the literature to compensate for the beam squint effect. One direct implementation of TTD elements is to replace the PS network with a TTD network, such that each antenna element is preceded by a dedicated TTD element [21]. However, such an implementation may not be energy-efficient, considering that the power consumption of a TTD element is almost three times that of a conventional PS [22], [23]. To this end, a hybrid analog precoder consisting of a TTD network and a PS network has been proposed, where the PS network is driven by a limited number of TTDs [24]–[26]. However, these works adopt impractical assumptions of unlimited maximum delay range and infinite-resolution TTDs, as well as infinite-resolution PSs.

A. Problem Statement and Related Work

Hardware constraints, such as the maximum delay range and time delay resolution of TTDs, along with the resolution of PSs, limit the hybrid analog precoder's performance. Specifically, wideband time delay networks are typically implemented using digitally controlled switchable delay lines, which have finite resolution [27], [28]. In addition, TTD elements can provide a bounded time delay range of up to several hundreds of picoseconds [27], [29]. Similarly, PSs are digitally controlled and thus have finite resolution [30]. Recent works in the literature, such as [24] and [25], do not consider these hardware limitations, relying on impractical unlimited-range and infinite-resolution TTDs and PSs. To improve energy efficiency, the authors in [31] proposed a dynamic-subarray with a fixed true-time-delay architecture, which requires long-range TTD elements.

The authors in [32] and [33] proposed a joint delay-phase precoding method, where the TTD network and PS network are jointly designed to approach the optimal analog precoder while considering the maximum delay range constraint of TTDs. This scheme outperforms DPP scheme in [25] in terms of array gain while adhering to the aforementioned constraint. However, this approach is not scalable, as the resulting array gain deteriorates as the number of antenna elements increases. Additionally, the authors of [33] assume infinite-resolution TTDs and PSs in the hybrid analog precoder's design, which is impractical, as discussed before. Therefore, practical finite-resolution and limited-range TTD elements, as well as finite-resolution PSs, should be considered in the hybrid analog precoder's design.

B. Contributions

In this work, we propose practical hybrid analog precoding schemes, which combat beam squint effect at one hand and comply with the hardware limitations of TTDs and PSs on the other hand. The main contributions of this work are summarized as follows.

- We propose the delta-delay-phase precoding (DDPP) architecture to enable wideband beamforming while considering the practical limitations of limited-range and time resolution of TTDs. In contrast to the conventional delay-phase precoding architecture [25], DDPP inserts TTD elements between successive subarrays so that the time delay applied to a signal in a particular subarray is achieved by a group of TTD elements instead of a dedicated TTD element. Additionally, the proposed scheme addresses time resolution constraints.
- We propose a hybrid practical precoding scheme, which jointly optimizes the TTD network and PS network considering their hardware limitations. Specifically, we formulate the design of the hybrid analog precoder as a non-convex joint optimization problem subjected to the resolution constraints of TTDs and PSs and also to the limited-range of TDDs. An alternating minimization is utilized to solve the optimization problem.
- To reduce the computational complexity of the hybrid practical precoding scheme, we propose a low-complexity precoding approach, which ensures a fixed value for all TTDs of the system, thereby significantly reducing computational overhead compared to the original hybrid practical precoding scheme.
- We carry out extensive simulations to verify the effectiveness of the proposed precoding architecture and the hybrid precoding schemes in dealing with the hardware limitations of TTDs and PSs compared to the state-of-art hybrid precoding approaches in the literature.

In this context, a preliminary investigation of the hybrid analog precoding under the hardware limitations of TTDs is presented in [1]. Our work in [1] primarily addresses the finite-resolution limitation of TTDs in the design of the hybrid analog precoder, whereas the maximum delay range of TTDs is considered as a constraint to the optimization problem. Nevertheless, the work in [1] suffers array gain loss as the maximum delay range supported by TTDs decreases. In the same vien, a remarkable gain loss occurs with the adoption of higher number of antenna elements, which makes the work in [1] unscalable for UM-MIMO systems. Moreover, the work in [1] doesn't consider the hardware limitations of PSs, where impractical infinite-resolution PSs are assumed.

The remainder of this paper is organized as follows. In Sec. II, we present the wideband channel model and an overview of beam squint effect and recent hybrid precoding approaches. In Sec. III, we introduce the proposed delta-delay-phase precoding (DDPP) architecture and present the time resolution constrained hybrid precoding (TR-HP). In Sec. IV, we propose the hybrid practical precoding (HPP), which accounts for the hardware limitations of TTDs and PSs. In Sec. V, we propose the fixed-delta hybrid practical precoding (FD-HPP), that features low computational complexity. Simulation results and discussions are presented in Sec. VI before concluding the paper in Sec. VII.

Notation: $\mathbf{A}$, $\mathbf{a}$, and a denote a matrix, a vector, and a scalar, respectively. $\mathbf{a}(i)$ is the i^{th} element of a vector $\mathbf{a}$ and $\mathbf{A}(i,j)$ is the element with the indicies i and j of a matrix $\mathbf{A}$ whereas $\mathbf{A}(i:j,:)$ is a submatrix of $\mathbf{A}$ from its i^{th} row to the j^{th} row. $[\mathbf{a} \mid \mathbf{b}]$ indicates the concatenation of $\mathbf{a}$ and $\mathbf{b}$. $\|\mathbf{A}\|_F$, $\mathbf{A}^*$,$\mathbf{A}^T$, $\mathbf{A}^H$ denote the Frobenius norm, conjugate, transpose, and Hermitian of a matrix $\mathbf{A}$, respectively. $\textbf{blkdiag}(\mathbf{a}_1, \mathbf{a}_2, ..., \mathbf{a}_n)$ represents a block diagonal matrix, whose blocks are $\mathbf{a}_1, \mathbf{a}_2, ..., \mathbf{a}_n$. $\mathbf{0}_{n,m}$ and $\mathbf{1}_n$ denote an $n \times m$ empty matrix and an n long all-ones vector, respectively. $\mathbf{I}_n$ denotes the $n \times n$ identity matrix. $\mathbf{QZ}_{\Upsilon}(x)$ function quantizes a real number x to the nearest element in set Υ. $\mathrm{Re}\{z\}$ and $\mathrm{ang}\{z\}$ return the real part and the angle of a complex number z, respectively. $\lfloor a \rceil$ rounds a real number a to the nearest integer and $\mathrm{sign}(a)$ returns the sign of a. $\min(a,b)$ returns the minimum of real numbers a and b. $\mathrm{Ln}(z)$ is the principle value for the natural logarithm $\ln(z)$ of a complex number z. $\preceq$ indicates the element-wise vector inequality. $\mathbb{C}$, $\mathbb{R}$, $\mathbb{Z}$, and $\mathbb{B}$ are the sets of complex numbers, real numbers, integers, and boolean, respectively.

II. Wideband Channel Model and Beam Squint Effect

A. Wideband Channel Model

We consider the downlink of a wideband UM-MIMO-OFDM system with M subcarriers such that the frequency of the m^{th} subcarrier is given by $f_m = f_c + \frac{B}{M}[m - \frac{M+1}{2}]$, where f_c and B indicate the carrier frequency and bandwidth, respectively. We denote $\mathbf{f} = [f_1, ..., f_M]^T \in \mathbb{R}^{M \times 1}$ as the subcarriers' vector. The base station (BS) is equipped with a uniform linear array (ULA) with N_{T} antenna elements serving U single-antenna mobile users. The communication channel is modeled using a geometrical approach, which accounts for the presence of L scatterers between the BS and the mobile users. Hence, the channel can be modeled as a sum of L distinct propagation paths such that the channel vector between the BS and the u^{th} mobile user at the m^{th} subcarrier

is expressed as

$$\mathbf{h}_{m,u} = \sqrt{\frac{N_T}{L}} \sum_{l=1}^{L} \alpha_{l,u} e^{-j2\pi\gamma_{l,u} f_m} \mathbf{a}^H(\Theta_m^{l,u}). \tag{1}$$

$\alpha_{l,u}$ and $\gamma_{l,u}$ are the complex path gain and path delay of the l^{th} path for the u^{th} user, respectively. $\mathbf{a}(\Theta_m^{l,u})$ is the response vector of the phased array at the m^{th} subcarrier, where $\Theta_m^{l,u}$ denotes the spatial frequency as follows

$$\Theta_m^{l,u} = \frac{2\pi f_m d}{v} \sin\theta_{l,u}, \tag{2}$$

where $d,\ v,$ and $\theta_{l,u} \in [-\pi/2, \pi/2]$ are the array interelement distance, the speed of light and the angle of departure (AoD) of the l^{th} path for the u^{th} user, respectively. The response vector of the phased array for a ULA at the m^{th} subcarrier is given as

$$\mathbf{a}(\Theta_m^{l,u}) = \frac{1}{\sqrt{N_T}} [1, e^{j\Theta_m^{l,u}}, ..., e^{j(N_T-1)\Theta_m^{l,u}}]^T. \tag{3}$$

In conclusion, the channel matrix $\mathbf{H}_m \in \mathbb{C}^{U \times N_T}$ between the BS and the U mobile users is expressed as

$$\mathbf{H}_m = [\mathbf{h}_{m,1}^T, ..., \mathbf{h}_{m,U}^T]^T. \tag{4}$$

B. Beam Squint Effect

Beam squint effect occurs as a consequence of using frequency-independent PSs in the analog part of wideband hybrid analog beamformers, which is denoted as PS-based precoding and described as

$$\mathbf{a}(\Theta_c^{l,u}) = \frac{1}{\sqrt{N_T}} [1, e^{j\Theta_c^{l,u}}, ..., e^{j(N_T-1)\Theta_c^{l,u}}]^T, \tag{5}$$

where $\Theta_c^{l,u}$ indicates the spatial frequency at f_c. From (5), we note that the response vector of the phased array is designed for the carrier frequency f_c and applied to the whole bandwidth. In consequence, margin subcarriers suffer array gain losses in comparison with the carrier frequency, where the normalized array gain at the m^{th} subcarrier for a given angle $\theta_{l,u}$ is expressed as

$$g_m(\theta_{l,u}) = |\mathbf{a}^H(\Theta_c^{l,u})\ \mathbf{a}(\Theta_m^{l,u})| = \frac{1}{N_{\text{T}}} \left| \sum_{n=1}^{N_{\text{T}}} e^{j(n-1)(\Theta_m^{l,u} - \Theta_c^{l,u})} \right|. \tag{6}$$

From (6), it is pretty clear that $g_m(\theta_{l,u}) = 1$ when $\Theta_m^{l,u} = \Theta_c^{l,u}$, namely when $f_m = f_c$. Meanwhile, $g_m(\theta_{l,u}) < 1$ when $f_m \neq f_c$. Accordingly, the optimal analog precoder required to combat squint effect over all subcarriers should be frequency-dependent as follows

$$\mathbf{C}_m^l = [\mathbf{c}_m^{l,1}, ..., \mathbf{c}_m^{l,U}], \tag{7}$$

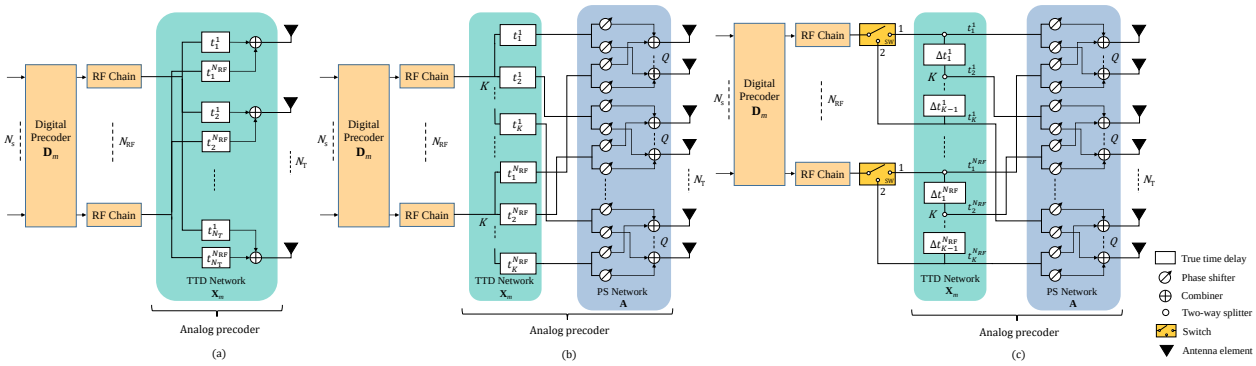

Fig. 1: Wideband hybrid precoding: (a) full-TTD precoding architecture (b) delay-phase precoding (DPP) architecture (c) the proposed delta-delay-phase precoding (DDPP) architecture.

where $\mathbf{c}_m^{l,u} = \mathbf{a}(\Theta_m^{l,u})$ represents the optimal analog precoder over the l^{th} path for the the u^{th} user at the m^{th} subcarrier. As a result, the optimal analog precoder is capable of achieving a unity array gain of $g_m(\theta_{l,u}) = |\mathbf{a}^H(\Theta_m^{l,u})\ \mathbf{a}(\Theta_m^{l,u})| = 1$ across all subcarriers, thereby eliminating the beam squint effect. However, implementing this precoder necessitates delay-controlled analog precoding instead of the conventional phase-controlled analog precoding. This entails embedding a dedicated TTD per antenna element in the RF front-end to enable wideband beamforming, as illustrated in Fig.1.a, which is denoted in this paper as full-TTD precoding. The implementation of full-TTD precoding can be impractical in terms of power consumption and hardware complexity, especially when a large number of TTDs are required. In consequence, DPP has been introduced as a compromise between performance and hardware complexity [25].

DPP technique employs a limited number of TTDs, where the antenna array is divided into K subarrays, each with $Q = N_{\text{T}}/K$ antenna elements controlled by a single TTD element as depicted in Fig.1.b. This configuration provides a practical system design while still approaching near-optimal performance, comparable to that of a full-TTD precoder.

Fig.2 displays the normalized array gain computed using (6) for the various precoding schemes mentioned earlier. The computation assumes half-wavelength spaced antennas with $f_c = 300$ GHz, $B = 30$ GHz, $M = 128$, $K = 16$, $N_{\text{T}} = 256$, and $\theta_{l,u} = 0.5$ rad. The results show that the full-TTD precoder achieves a constant normalized gain across all subcarriers, while the normalized gain of the PS-based precoder decreases as the subcarrier frequency moves away from the carrier frequency. In contrast, DPP demonstrates near-optimal performance with significantly reduced hardware complexity compared to the full-TTD precoder.

DPP requires time delay values that scale up with the TTD's index. Specifically, the time

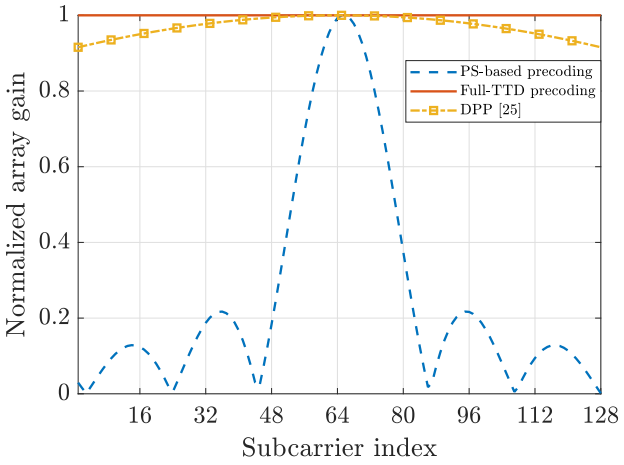

Fig. 2: Normalized array gain versus subcarriers when $N_{\mathrm{T}} = 256$.

delay value of the k^{th} TTD belonging to the n^{th} RF chain is given as [25]

$$t_k^n = -(k-1)Q\frac{d}{v}\sin\theta_{l,u} \;\forall\; k = 1, 2, .., K. \tag{8}$$

For instance, the required time delay range is nearly 1.7 ns when $K = 16$ and $\theta_{l,u} = \pi/2$. This time delay is considerably higher than the time delay range attainable with state-of-the-art TTDs, i.e. around 500 ps [29]. The authors in [33] proposed joint DPP that satisfies the maximum time delay constraint of TTDs. This approach outperforms DPP [25] under the adoption of limited-range TTDs. However, the performance of this approach deteriorates as the number of antennas increases, which make it unsuitable for UM-MIMO systems. Moreover, this work assumes impractical infinite-resolution TTDs and PSs. However, in practical wideband communication systems, practical low-resolution TTDs and PSs are more appropriate to balance energy efficiency and performance [34]. Building upon the architecture proposed in [35] for angular coverage expansion, we propose next the delta-delay-phase precoding architecture that guarantees scalability for UM-MIMO systems, even with practical finite-resolution and limited-range TTDs.

III. Delta-Delay-Phase Precoding under True Time Delay Constraints

In this section, we present the proposed precoding architecture, which enables wideband beamforming in UM-MIMO systems using practical TTDs with limited range and finite resolution.

A. The proposed System Model

The required phase shift between adjacent subarrays in order to combat beam squint effect at the m^{th} subcarrier is given as [36]

$$\Delta\vartheta_m = Q\frac{2\pi d}{\lambda_m}\sin\theta_{l,u}, \tag{9}$$

where λ_m is the wavelength of the m^{th} subcarrier. Consequently, the required time delay difference between adjacent subarrays is derived by matching the phase shift obtained from a TTD element ψ_m to that in (9) as follows

$$\psi_m = -2\pi f_m \Delta t_k^n = -\frac{2\pi v}{\lambda_m}\Delta t_k^n \triangleq Q\frac{2\pi d}{\lambda_m}\sin\theta_{l,u}, \tag{10}$$

where Δt_k^n denotes the required time delay difference between the $(k+1)^{\text{th}}$ and k^{th} subarrays of the n^{th} RF chain. Consequently, the required time delay difference between adjacent subarrays of a given RF chain is given as

$$\Delta t_k^n = -Q\frac{d}{v}\sin\theta_{l,u} \;\forall\; k = 1, 2, ., K-1. \tag{11}$$

Observing (11), we note that the time delay difference between adjacent subarrays remains constant, provided that they have the same size, i.e., the same number of antenna elements Q. Building on this observation, we propose a novel architecture for hybrid analog precoding, where TTDs are inserted between neighboring subarrays, as illustrated in Fig.1.c. We refer to this proposed architecture as the delta-delay-phase precoding (DDPP) architecture, where the time delay difference between adjacent subarrays serves as the key optimization variable of interest in the TTD network. The RF signal is fed to successive subarrays through two-way splitters with cumulative time delays. Particularly, the time delay value applied on the signal fed to the k^{th} subarray of the n^{th} RF chain is realized by a set of TTDs $t_k^n = \sum_{i=1}^{k-1}\Delta t_i^n = \Delta t_1^n + \Delta t_2^n + ... + \Delta t_{k-1}^n$ rather than by a dedicated TTD as in [25], where Δt_i^n as a function of the time delay values over subarrays is given as

$$\Delta t_i^n = t_{i+1}^n - t_i^n \;\forall\; i \in 1, 2, ., K-1. \tag{12}$$

In contrast, the proposed DDPP architecture aims at alleviating the maximum time delay limitation of TTDs. Specifically, the DDPP architecture can surpass the maximum time delay of a single TTD element, by utilizing multiple TTDs in a stepwise manner. By implementing time delays between adjacent subarrays, the maximum delay limitation is imposed on the inter-subarray time delay difference instead of the time delay needed per subarray, thereby alleviating the burden on TTDs. Specifically, in comparison with (8), the proposed architecture achieves a reduction in the maximum delay range by a factor of $K-1$. Accordingly, we define $\mathbf{t}_n^{\triangle} = [\Delta t_1^n, \Delta t_2^n, ..., \Delta t_{K-1}^n] \in \mathbb{R}^{K-1\times 1}$ as the time delay vector of TTDs belonging to the n^{th} RF chain of the DDPP architecture. Meanwhile, $\mathbf{t}_n = [t_1^n, t_2^n, ..., t_K^n] \in \mathbb{R}^{K\times 1}$ denotes the resulting time delays over subarrays such that $\mathbf{t}_n \preceq \mathbf{1}_K t_{\text{req}}$, where $t_{\text{req}} = A_{\text{phys}}/v$ and A_{phys} indicate the maximum required time delay over subarrays and the array physical aperture, respectively [37].

Consequently, as the time delay difference between adjacent subarrays is fixed as depicted in (11), the time delay vector of TTDs belonging to the n^{th} RF chain is expressed as

$$\mathbf{t}_n^{\triangle} = -Q\frac{d}{v}\sin\theta_{l,u}\mathbf{1}_{K-1}. \tag{13}$$

As demonstrated in (13), the values of $\mathbf{t}_n^{\triangle}$ depend on $\theta_{l,u}$ and can be either positive or negative. However, TTD elements can not generate negative time delays. Thus, we propose inserting a 2-output switch between each RF chain and its corresponding analog precoder. This switch routes the signal to the first subarray through its 1^{st} output when the elements of $\mathbf{t}_n^{\triangle}$ are positive, which occurs when $\theta_{l,u} \in [-\pi/2, 0]$. It rather closes the 2^{nd} output feeding the signal to the last subarray first in case the elements of $\mathbf{t}_n^{\triangle}$ are negative, which occurs when $\theta_{l,u} \in [0, \pi/2]$. We model this switch as a binary selecting vector $\mathbf{e}$ as follows

$$\mathbf{e}(\theta_{l,u}) = \frac{1}{2|\sin(\theta_{l,u})|}\begin{bmatrix} |\sin(\theta_{l,u})| + \sin(\theta_{l,u}) \\ |\sin(\theta_{l,u})| - \sin(\theta_{l,u}) \end{bmatrix}. \tag{14}$$

The delta-based time delay vector over subarrays of the n^{th} RF chain when $\theta_{l,u} \in [-\pi/2, 0]$ is given as

$$\mathbf{t}_n^{+} = \begin{bmatrix} 0, \Delta t_1^n, ..., \sum_{k=1}^{K-1} \Delta t_k^n \end{bmatrix}^T, \tag{15}$$

where the first element of $\mathbf{t}_n^{+}$ is zero, since the RF-signal is fed to the first subarray with no time delay in the proposed DDPP architecture. Likewise, the delta-based time delay vector over subarrays of the n^{th} RF chain when $\theta_{l,u} \in [0, \pi/2]$ is given as $\mathbf{J}\mathbf{t}_n^{+}$, where $\mathbf{J} \in \mathbb{B}^{K\times K}$ denotes the permutation matrix with antidiagonal elements set to one and all other elements set to zero. Consequently, the resulting time delays over subarrays of the n^{th} RF chain is given as

$$\mathbf{t}_n = [\mathbf{t}_n^{+} \quad \mathbf{J}\mathbf{t}_n^{+}]\mathbf{e}(\theta_{l,u}). \tag{16}$$

The proposed DDPP architecture adopts hybrid precoding, where a PS network is embedded in the analog precoder as shown in Fig.1.c. We assume that the PS network is designed for the carrier frequency using (5). Consequently, the total phase difference between adjacent subarrays resulting from the TTD network and the PS network at the m^{th} subcarrier is expressed as

$$\tilde{\Delta}\vartheta_m = \underbrace{Q\frac{2\pi d}{\lambda_m}\sin\theta_{l,u}}_{\text{(a)}} + \underbrace{Q\frac{2\pi d}{\lambda_c}\sin\theta_{l,u}}_{\text{(b)}}. \tag{17}$$

We note from (17) that the phase difference between adjacent subarrays is composed of two

terms: (a) and (b). Particularly, term (a) in (17) represents the frequency-dependent phase difference required to combat beam squint effect, whereas term (b) denotes a fixed phase difference delivered by the PS network. Aiming at realizing the required phase shift difference between adjacent subarrays given in (9), we need to compensate term (b) in (17). To this end, we propose to adapt the phase shifts of the PS network to cancel the resulting inter-subarray phase difference. As term (b) corresponds to $-2\pi f_c \Delta t_k^n$, we propose to adjust the values of the PS network to attain a compensation phase difference of $+2\pi f_c \Delta t_k^n$, such that the resulting PS network based inter-subarray phase difference is nullified. This can be equalized by adding a phase shift of $+2\pi f_c t_k^n$ per subarray such that the phased array steering vector of the k^{th} subarray belonging to the n^{th} RF chain $\mathbf{a}_{n,k}$ is given as

$$\mathbf{a}_{n,k} = \bar{\mathbf{a}}_{n,k} e^{+j2\pi f_c t_k^n} \ \forall \ k \in 1, 2, ., K. \tag{18}$$

$\bar{\mathbf{a}}_{n,k}$ denotes the phased array steering vector of the k^{th} subarray belonging to the n^{th} RF chain, which is designed for the carrier frequency as follows

$$\bar{\mathbf{a}}_{n,k} = \frac{1}{\sqrt{N_T}} [e^{j(k-1)Q\Theta_c^{l,u}}, ..., e^{j(kQ-1)\Theta_c^{l,u}}]^T \ \forall \ k \in 1, 2, ., K. \tag{19}$$

Consequently, the PS network for N_{RF} RF chains $\mathbf{A} \in \mathbb{C}^{N_T \times KN_{\text{RF}}}$ is modeled as

$$\mathbf{A} = [\mathbf{blkdiag}(\mathbf{a}_{1,1}, .., \mathbf{a}_{1,K}), .., \mathbf{blkdiag}(\mathbf{a}_{N_{\text{RF}},1}, .., \mathbf{a}_{N_{\text{RF}},K})], \tag{20}$$

where $\mathbf{a}_n = [\mathbf{a}_{n,1}^T, ..., \mathbf{a}_{n,K}^T]^T \in \mathbb{C}^{N_{\text{T}} \times 1}$ represents the phased array steering vector of the n^{th} RF chain. The corresponding TTD network $\mathbf{X}_m \in \mathbb{C}^{KN_{\text{RF}} \times N_{\text{RF}}}$ at the m^{th} subcarrier is modeled as

$$\mathbf{X}_m = \mathbf{blkdiag}(\mathbf{x}_m^1, .., \mathbf{x}_m^{N_{\text{RF}}}). \tag{21}$$

Based on the proposed hybrid analog precoder, the received symbol vector $\mathbf{y}_m \in \mathbb{C}^{N_{\text{s}} \times 1}$ at the m^{th} subcarrier is given by

$$\mathbf{y}_m = \mathbf{H}_m \mathbf{A} \mathbf{X}_m \mathbf{D}_m \mathbf{s}_m + \mathbf{n}_m, \tag{22}$$

where $\mathbf{s}_m \in \mathbb{C}^{N_{\text{s}} \times 1}$ represents the input symbol vector, and N_{s} denotes the number of data streams. $\mathbf{D}_m \in \mathbb{C}^{N_{\text{RF}} \times N_s}$ indicates the digital precoder at the m^{th} subcarrier, and $\mathbf{n}_m \in \mathbb{C}^{U \times 1}$ denotes the complex additive white Gaussian noise (AWGN) vector with zero mean and σ_{noise}^2 variance.

In conclusion, the design of the hybrid precoding scheme proposed in this work is summarized in (13) and (18), wherein the elements of $\mathbf{t}_n^{\triangle}$ are upperbounded by $t_{\max}$. Thanks to the DDPP architecture, the proposed precoding scheme effectively reduces the maximum time delay required from TTDs by a factor of $K-1$. In consequence, the proposed architecture offers high degree of practicality for UM-MIMO systems, where a large number of TTDs is needed, as the

severity of beam squint effect is directly proportional to the number of antenna elements [36].

B. True Time Delay Resolution Constraint

The resolution of TTDs is an additional hardware limitation on the hybrid precoder, where time delay networks are commonly realized by time delay elements connected through switchable delay lines. This implementation imposes a finite resolution constraint on the time delay values realized by these networks. Therefore and aiming at a practical system design, the resolution constraint of TTDs should be taken into account in the design of the hybrid analog precoder. In this subsection, we propose a hybrid analog precoding scheme to address this limitation.

We analyze the time resolution error that occurs due to the adoption of finite-resolution TTDs considering the time delay vector $\mathbf{t}_n$ at the output of the TTD network. The time resolution error results from rounding the required time delay value to an integer multiple of the time delay resolution t_{res}. The time resolution error of the time delay value over the k^{th} subarray belonging to the n^{th} RF chain is given as

$$\tau_k^n = t_k^n - \lfloor \frac{t_k^n}{t_{\text{res}}} \rceil t_{\text{res}}. \tag{23}$$

After considering the time delay resolution constraint, the time delay vector $\mathbf{t}_n$ is expressed as

$$\mathbf{t}_n = \left[\lfloor \frac{t_1^n}{t_{\text{res}}} \rceil t_{\text{res}}, \lfloor \frac{t_2^n}{t_{\text{res}}} \rceil t_{\text{res}}, ..., \lfloor \frac{t_K^n}{t_{\text{res}}} \rceil t_{\text{res}} \right]^T. \tag{24}$$

Since a TTD element delivers frequency-dependent phase shifts, it also produces frequency-dependent phase errors due to the time resolution error. Therefore, we propose to convert the time error resulted from the time delay resolution into a phase error, which we compensate for by introducing an equalization phase shift to the PS network. We can model the time resolution error τ_k^n as a vector of frequency-dependent phase errors $\boldsymbol{\varphi}_k^n \in \mathbb{R}^{M\times 1}$ expressed as

$$\boldsymbol{\varphi}_k^n = -2\pi \mathbf{f} \tau_k^n = \begin{pmatrix} \varphi_{k,1}^n \\ . \\ . \\ \varphi_{k,M}^n \end{pmatrix}, \tag{25}$$

where $\varphi_{k,m}^n$ denotes the phase error resulted at the m^{th} subcarrier due to the time delay resolution. We propose to compensate these phase shift errors by adding equalization phase shifts ϕ_k^n to the PS network. We model this optimization problem as the minimization of the squared frobenius norm of the sum of the phase errors $\boldsymbol{\varphi}_k^n$ and the equalization phase ϕ_k^n for a given subarray.

Accordingly, the problem is formulated as

$$\text{P1:} \min_{\phi_k^n} \|-2\pi \mathbf{f}\tau_k^n + \phi_k^n\|_F^2. \tag{26}$$

Let's define $\phi_k^n = 2\pi\rho_k^n\tau_k^n$, where ρ_k^n is an auxilliary optimization variable corresponding to the equalization phase ϕ_k^n. Accordingly, Problem P1 can be rewritten as

$$\text{P2:} \min_{\rho_k^n} \left\| -2\pi \begin{pmatrix} f_1 - \rho_k^n \\ . \\ . \\ f_M - \rho_k^n \end{pmatrix} \tau_k^n \right\|_F^2, \tag{27}$$

where Problem P2 can be simplified to

$$\text{P3:} \min_{\rho_k^n} \sum_{m=1}^{M} (\rho_k^n - f_m)^2. \tag{28}$$

By substituting $f_m = f_c + \frac{B}{M}[m - \frac{M+1}{2}]$, the objective function of Problem P3 can be expressed as

$$\sum_{m=1}^{M} \left[\rho_k^n - f_c - \frac{B}{M}\left(m - \frac{M+1}{2}\right)\right]^2. \tag{29}$$

Following linear algebra, Problem P3 can be rewritten as

$$\text{P4:} \min_{\rho_k^n} \left[M\rho_k^{n2} - 2Mf_c\rho_k^n + f_c^2 M + \left(\frac{B}{M}\right)^2 \left(\frac{-2M^3 - 3M^2 + 6M + 3}{12}\right)\right]. \tag{30}$$

We obtain the value of ρ_k^n that solves Problem P4 by setting the derivative of the objective function in P4 with respect to ρ_k^n to zero. This can be expressed as follows

$$2M\rho_k^n + -2Mf_c = 0. \tag{31}$$

As a result of (31), $\rho_k^n = f_c$, and, accordingly, the corresponding equalization phase is $\phi_k^n = 2\pi f_c \tau_k^n$. The equalization phase ϕ_k^n is added to the corresponding subarray, resulting in an adjusted phased array steering vector as

$$\mathbf{a}_{n,k} = \bar{\mathbf{a}}_{n,k}.e^{+j2\pi f_c[t_k^n + \tau_k^n]} \ \forall \ k \in 1, 2, .., K. \tag{32}$$

We determine the time delay vector $\mathbf{t}_n^{\triangle}$ for the DDPP architecture by substituting (24) in (12). The elements of $\mathbf{t}_n^{\triangle}$ are then upperbounded by $t_{\max}$ to comply with the maximum delay range constraint of TTDs. The switch closes to its first output if $\mathbf{t}_n^{\triangle} \succeq \mathbf{0}_{K-1,1}$, otherwise it closes to the second output. We denote this precoding scheme as the time resolution constrained hybrid precoding (TR-HP).

The proposed DDPP based TR-HP effectively addresses the hardware limitations of TTDs,

enabling practical implementation of wideband beamforming under TTD contraints.

IV. Hybrid Analog Precoding under True Time Delay and Phase Shifter Constraints

In the preceding section, we propose hybrid precoding schemes that incorporate practical finite-resolution and limited-range TTDs with infinite-resolution PSs. In the same vein, recent works in the literature have also used infinite-resolution PSs in the development of hybrid analog precoders [25], [32], [33], which is impractical due to the associated cost and power consumption in UM-MIMO systems. Therefore, in this part, we propose a hybrid analog precoding scheme that accounts for both TTD and PS hardware limitations, which we denote as the hybrid practical precoding (HPP). The problem of interest is to design the elements of $\mathbf{t}_n$ and $\mathbf{A}$ in order to minimize the Euclidean distance between the optimal analog precoder $\mathbf{C}_m$ and the resulting hybrid precoder over all subcarriers subjected to low-resolution TTDs and PSs constraints. We hereby confine the optimization domain of $\mathbf{t}_n$ to a set of discrete time delay values Υ, where the elements of Υ are integers multiple of the time delay resolution $t_{\rm res}$. Similarly, non-zero elements of $\mathbf{A}$ belong to a set Γ, which contains quantized phase shifts with constant modulus $\frac{1}{\sqrt{N_{\rm T}}}$. Accordingly, the problem is formulated as

$$\text{P5:}\ \underset{\mathbf{A},\{\mathbf{t}_n\}_{n=1}^{N_{RF}}}{\text{minimize}} \sum_{m=1}^{M} \left\|\mathbf{C}_m - \mathbf{A}\mathbf{X}_m(\{\mathbf{t}_n\}_{n=1}^{N_{RF}})\right\|_F^2, \tag{33a}$$

$$\mathbf{s.t.}\ \ \mathbf{A}(w,r) \in \{0,\Gamma\}\ \forall\ w \in 1,2,.,N_{\rm T},\ \ r \in 1,2,.,KN_{\rm RF}, \tag{33b}$$

$$t_k^n \in \Upsilon\ \forall\ n \in 1,2,..,KN_{\rm RF},\ \ k \in 1,2,.,K. \tag{33c}$$

The constraint (33b) indicates the sparsity of $\mathbf{A}$, whose elements are either zeros or belong to Γ. The constraint (33c) denotes the time delay resolution imposed on the elements of $\mathbf{t}_n$.

The objective function of Problem P5 in (33a) is equivalently written as

$$\sum_{m=1}^{M}\sum_{n=1}^{N_{\rm RF}}\sum_{k=1}^{K} \left\|\mathbf{c}_{n,k,m} - \mathbf{a}_{n,k}e^{-j2\pi f_m t_k^n}\right\|_F^2, \tag{34}$$

where $\mathbf{c}_{n,k,m} \in \mathbb{C}^{Q\times 1}$ is a subvector of the $n^{\rm th}$ column of $\mathbf{C}_m$ corresponding to the $k^{\rm th}$ subarray.

By introducing $\mathbf{b}(t_k^n) = e^{-j2\pi \mathbf{f} t_k^n} \in \mathbb{C}^{M\times 1}$ as the phase shifts' vector resulting from the time delay value t_k^n over M subcarriers, the objective function in (34) can be rewritten as

$$\sum_{n=1}^{N_{\rm RF}}\sum_{k=1}^{K} \left\|\mathbf{C}_{n,k} - \mathbf{a}_{n,k}\mathbf{b}^T(t_k^n)\right\|_F^2, \tag{35}$$

where $\mathbf{C}_{n,k} = [\mathbf{c}_{n,k,1},...,\mathbf{c}_{n,k,M}] \in \mathbb{C}^{Q\times M}$. From (35), we can conclude that our problem in P5 is equivalent to the minimization of the contribution of each subarray and its time delay value

to the overall objective function. Hence, Problem P5 can be divided into KN_{RF} subproblems, where each subproblem handles the joint optimization between the time delay value and phase shifts of a given subarray. We formulate the joint optimization subproblem of the k^{th} subarray belonging to the n^{th} RF chain subjected to the time delay and phase shift resolutions as

$$\text{P6:} \ \underset{\mathbf{a}_{n,k},t_k^n}{\text{minimize}} \left\| \mathbf{C}_{n,k} - \mathbf{a}_{n,k}\mathbf{b}^T(t_k^n) \right\|_F^2, \tag{36a}$$

$$\mathbf{s.t.} \ \ \mathbf{a}_{n,k}(q) \in \Gamma \ \forall \ q = 1, 2, ., Q, \tag{36b}$$

$$t_k^n \in \Upsilon. \tag{36c}$$

Problem P6 relieves the sparsity limitation imposed on the optimization variables of Problem P5, where $\mathbf{a}_{n,k}$ and $\mathbf{b}(t_k^n)$ are non-sparse variables. However, this joint optimization problem is intractable, where non-convex constraints (36b) and (36c) hinder finding a global optimal solution. Therefore, we propose next an iterative optimization using alternating minimization in order to handle such NP-hard problem [38].

Alternating minimization is a common practice to solve such non-convex optimization problems with several types of variables. Therefore, we propose an alternating minimization based iterative algorithm to find a local optimal solution to Problem P6. Specifically, the joint optimization problem in P6 is decoupled into two problems. The first problem P7 optimizes PS precoding vector $\mathbf{a}_{n,k}$ while t_k^n is fixed, which is formulated as

$$\text{P7:} \ \underset{\mathbf{a}_{n,k}}{\text{minimize}} \left\| \mathbf{C}_{n,k} - \mathbf{a}_{n,k}\mathbf{b}^T(t_k^n) \right\|_F^2, \tag{37a}$$

$$\mathbf{s.t.} \ \ \mathbf{a}_{n,k}(q) \in \Gamma \ \forall \ q = 1, 2, .., Q. \tag{37b}$$

The second problem P8 optimizes t_k^n while $\mathbf{a}_{n,k}$ is fixed, which is formulated as

$$\text{P8:} \ \underset{t_k^n}{\text{minimize}} \left\| \mathbf{C}_{n,k} - \mathbf{a}_{n,k}\mathbf{b}^T(t_k^n) \right\|_F^2, \tag{38a}$$

$$\mathbf{s.t.} \ \ t_k^n \in \Upsilon. \tag{38b}$$

By temporarily neglecting the constraint (37b), Problem P7 has an optimal solution given as

$$\mathbf{a}_{n,k} = \frac{1}{M}\mathbf{C}_{n,k}\mathbf{b}^*(t_k^n). \tag{39}$$

Similarly, by temporarily neglecting the constraint (38b), Problem P8 has an optimal solution for $\mathbf{b}(t_k^n)$ given as

$$\mathbf{b}(t_k^n) = \frac{N_{\mathrm{T}}}{Q}(\mathbf{a}_{n,k}^H\mathbf{C}_{n,k})^T. \tag{40}$$

However, we still need to derive the time delay value t_k^n corresponding to $\mathbf{b}(t_k^n)$. Knowing that

$\mathbf{b}(t_k^n) = e^{-j2\pi \mathbf{f} t_k^n}$, we can write

$$\ln[\mathbf{b}(t_k^n)] = -j2\pi \mathbf{f} t_k^n. \tag{41}$$

Consequently, time delay value t_k^n can be isolated as [39]

$$t_k^n = \mathrm{Re}\left\{ \frac{1}{-j2\pi \sum_{m=1}^{M} f_m^2} \mathbf{f}^* \{\mathrm{Ln}[\mathbf{b}(t_k^n)] + jp2\pi\} \right\}, \tag{42}$$

where $p \in \mathbb{Z}$. Since the complex exponential function is periodic with a period of $j2\pi$, its complex logarithm is described as multi-valued function. Particularly, (42) holds as a solution for any imaginary number $j2\pi p$ added to its logarithmic expression. Therefore, we propose to perform a one-dimensional search over a probing integer $p \in [-\xi, \xi]$ to find the time value t_k^n that solves Problem P9, which is formulated as

$$\text{P9:} \ \underset{t_k^n}{\text{minimize}} \left\| e^{-j2\pi \mathbf{f} t_k^n} - \mathbf{b}(t_k^n) \right\|_F^2. \tag{43}$$

The value of p corresponding to the searched time value t_k^n is directly proportional to the subcarrier frequency and maximum required time delay over subarrays. Therefore, a search limit is recommended to be $\xi = f_M t_{\mathrm{req}}$. The proposed procedure is summarized in Algorithm 1.

Algorithm 1: Finding time delay value

Input: $\mathbf{b}(t_k^n),\ \mathbf{f}$

Output: t_k^n

Initialization: $i = 0$, $\Omega = 10^6$

for $p = -\xi \ ... \ \xi$ **do**

  $i = i + 1$

  t_i=Re$\left\{ \frac{1}{-j2\pi \sum_{m=1}^{M} f_m^2} \mathbf{f}^* [\mathrm{Ln}[\mathbf{b}(t_k^n)] + jp2\pi] \right\}$

  if $(\left\| e^{-j2\pi \mathbf{f} t_i} - \mathbf{b}(t_k^n) \right\|_F^2 < \Omega)$ **then**

    $\Omega = \left\| \ e^{-j2\pi \mathbf{f} t_i} - \mathbf{b}(t_k^n) \right\|_F^2$

    update $t_k^n \leftarrow t_i$

  end if

end for

return t_k^n

Algorithm 2: Hybrid practical precoding (HPP)

Input: $\mathbf{f},\ \mathbf{C}_n^{\star},\ \Upsilon,\ N_{\mathrm{T}},\ Q,\ M,\ Iter, \epsilon$

Output: $\mathbf{a}_n, \mathbf{t}_n, \mathbf{t}_n^{\triangle}$

Initialization: $\mathbf{a}_n = \mathbf{0}_{N_{\mathrm{T}},1}, \mathbf{t}_n = \mathbf{0}_{K,1}, \mathbf{t}_n^{\triangle} = \mathbf{0}_{K-1,1}$

Parallel for $k = 1 : K$ **do**

  $i = 0$

  $\mathbf{F}_{n,k}^{0} = \mathbf{0}_{Q,M}$

  $\tilde{\mathbf{a}}_{n,k} = \dfrac{1}{\sqrt{N_{\mathrm{T}}}}\mathbf{1}_Q$

  $\mathbf{C}_{n,k} = \mathbf{C}_n^{\star}((k-1)Q + 1 : kQ, :)$

  while *true* **do**

    $i = i + 1$

    update $\mathbf{b}(t_k^n) \leftarrow \dfrac{N_{\mathrm{T}}}{Q}(\tilde{\mathbf{a}}_{n,k}^H \mathbf{C}_{n,k})^T$

    $t_k^n = \text{Algorithm1}[\mathbf{b}(t_k^n)]$

    $\tilde{t}_k^n = \mathbf{QZ}_{\Upsilon}(t_k^n)$

    update $\mathbf{a}_{n,k} \leftarrow \dfrac{1}{M}\mathbf{C}_{n,k}\mathbf{b}^*(\tilde{t}_k^n)$

    $\tilde{\mathbf{a}}_{n,k} = \mathbf{QZ}_{\Gamma}(\mathbf{a}_{n,k})$

    $\mathbf{F}_{n,k}^{i} = \ \tilde{\mathbf{a}}_{n,k}\mathbf{b}^T(\tilde{t}_k^n)$

    if $(\left\| \ \mathbf{F}_{n,k}^{i} - \mathbf{F}_{n,k}^{i-1} \right\|_F^2 < \epsilon \parallel i = Iter)$ **then**

      $\mathbf{a}_n = [\mathbf{a}_n \mid \tilde{\mathbf{a}}_{n,k}]$

      $\mathbf{t}_n = [\mathbf{t}_n \mid \tilde{t}_k^n]$

    end if

    break

  end while

end for

Parallel for $k = 1 : K - 1$ **do**

  $\Delta t_k^n = \text{sign}(\tilde{t}_{k+1}^n - \tilde{t}_k^n)\min(|\tilde{t}_{k+1}^n - \tilde{t}_k^n|, t_{max})$

  $\mathbf{t}_n^{\triangle} = [\mathbf{t}_n^{\triangle} \mid \Delta t_k^n]$

end for

return $\mathbf{a}_n, \mathbf{t}_n, \mathbf{t}_n^{\triangle}$

Now, we propose a joint iterative optimization algorithm to solve problems in P7 and P8 alternately with the consideration of constraints (37b) and (38b). The iterative optimization starts by initializing the phased array vector $\mathbf{a}_{n,k}$ as an all-ones vector scaled by a constant modulus $1/\sqrt{N_{\mathrm{T}}}$. Based on $\mathbf{a}_{n,k}$, the phase shifts vector over subcarriers $\mathbf{b}(t_k^n)$ is calculated using (40). Afterwards, the resulting vector is passed to Algorithm 1 to find the corresponding time delay value t_k^n. Subsequently, the resulting time value is quantized to the nearest element in Υ to satisfy (38b). Based on the resulting time value $\tilde{t}_k^n$, the phased array vector $\mathbf{a}_{n,k}$ is updated using (39) and the elements of the resulting vector are quantized to the nearest phase shifts in Γ to satisfy (37b). These steps are iteratively performed until convergence. The convergence is met once the Euclidean distance between the actual hybrid precoder per subarray $\mathbf{F}_{n,k}^{i}$ and that resulted in the previous iteration $\mathbf{F}_{n,k}^{i-1}$ is lower than a threshold ϵ or by reaching the maximum number of iterations, i.e. $Iter$. The time delay vector of TTDs for the DDPP architecture $\mathbf{t}_n^{\triangle}$ is determined using (12). The maximum delay range constraint is imposed on the elements of $\mathbf{t}_n^{\triangle}$, where the elements of $\mathbf{t}_n^{\triangle}$ are upperbounded by $t_{\max}$. The switch closes to the first output if $\mathbf{t}_n^{\triangle} \succeq \mathbf{0}_{K-1,1}$, while it closes to the second output otherwise. The proposed algorithm is executed in parallel on subarrays' level of a specific RF chain and scaled up to multiple RF chains. The proposed algorithm is summarized in Algorithm 2 where $\mathbf{C}_n^{\star} = [\mathbf{C}_{n,1}^T, ..., \mathbf{C}_{n,K}^T]^T \in \mathbb{C}^{N_{\mathrm{T}} \times M}$ denotes the full-TTD precoder of subarrays belonging to the n^{th} RF chain.

V. Fixed-delta hybrid practical precoding

The proposed hybrid practical precoding scheme addresses the resolution constraints of TTDs and PSs. However, it does not ensure identical inter-subarray time delay differences across all subarrays, which is desirable for practical cost-efficient design [35]. Therefore, we propose customizing HPP scheme to ensure both identical inter-subarray time delay differences and reduced computational complexity. We denote this precoding scheme as the fixed-delta hybrid practical precoding (FD-HPP). We confine Problem P6 to the first pair of subarrays as follows

$$\text{P10:} \quad \underset{\mathbf{a}_{n,k}, t_k^n}{\text{minimize}} \left\| \mathbf{C}_{n,k} - \mathbf{a}_{n,k} \mathbf{b}^T(t_k^n) \right\|_F^2, \tag{44a}$$

$$\mathbf{s.t.} \quad \mathbf{a}_{n,k}(q) \in \Gamma \ \forall \ q = 1, 2, .., Q, \ \ k = 1, 2, \tag{44b}$$

$$t_k^n \in \Upsilon \ \forall \ k = 1, 2. \tag{44c}$$

We derive the time delay values for the first two subarrays by solving Problem P10 in the same iterative manner as for Problem P6 in (36a). Based on the derived time delay values t_1^n and t_2^n,

we calculate the inter-subarray time delay value between the first pair of subarrays as

$$\Delta t_1^n = t_2^n - t_1^n. \tag{45}$$

We adopt this inter-subarray time delay value for all successive TTDs such that the time delay vector of TTDs belonging to n^{th} RF chain is expressed as

$$\mathbf{t}_n^{\triangle} = \Delta t_1^n \mathbf{1}_{K-1}. \tag{46}$$

The switch closes to the first output if $\Delta t_1^n \geq 0$, while it closes to the second output otherwise. The corresponding phase shifts are calculated using (39) and subsequently quantized to the nearest elements in Γ. The proposed algorithm, which is summarized in Algorithm 3, guarantees identical inter-subarray time delay differences while maintaining lower computational overhead.

Algorithm 3: Fixed-delta hybrid practical precoding (FD-HPP)

Input: $\mathbf{f},\ \mathbf{C}_n^{\star},\ t_{\max},\ N_T,\ Q,\ M,\ Iter, \epsilon$

Output: $\mathbf{a}_n, \mathbf{t}_n, \mathbf{t}_n^{\triangle}$

1 **Initialization:**

2 $\mathbf{a}_n = \mathbf{0}_{N_T,1}, \mathbf{t}_n = \mathbf{0}_{K,1}, \mathbf{t}_n^{\triangle} = \mathbf{0}_{K-1,1}$

3 **Parallel for** $k = 1:2$ **do**

4 Perform steps (3-20) of Algorithm 2

5 **end for**

6 $\Delta t_1^n = \tilde{t}_2^n - \tilde{t}_1^n$

7 $\mathbf{t}_n^{\triangle} = \Delta t_1^n \mathbf{1}_{K-1}$

8 $\mathbf{t}_n = [0, 1, ..., K-1]^T \Delta t_1^n$

9 **Parallel for** $k = 3:K$ **do**

10 $\mathbf{C}_{n,k} = \mathbf{C}_n^{\star}((k-1)Q + 1 : kQ, :)$

11 $\tilde{\mathbf{a}}_{n,k} = \mathbf{Q}\mathbf{Z}_{\Gamma}[\frac{1}{M}\mathbf{C}_{n,k} e^{j2\pi \mathbf{f} t_k^n}]$

12 $\mathbf{a}_n = [\mathbf{a}_n \mid \tilde{\mathbf{a}}_{n,k}]$

13 **end for**

14 **return** $\mathbf{a}_n, \mathbf{t}_n, \mathbf{t}_n^{\triangle}$

The computational complexity of HPP is dominated by steps 9, 10, 12, and 14. In specific, the complexity of steps 9, 12, and 14 is $\mathcal{O}(M.Q)$ whereas the complexity of step 10, i.e. Algorithm 1, is $\mathcal{O}(\xi.M)$. As HPP runs for $Iter$ iterations per subarray, it has a complexity of

$[\mathcal{O}(K.Iter.M.Q) + \mathcal{O}(K.Iter.\xi.M)]$. On the other hand, the proposed FD-HPP features lower computational overhead with a factor of K where the iterative loop runs only for the first two subarrays. Therefore, it has a complexity of $[\mathcal{O}(Iter.M.Q)+\mathcal{O}(Iter.\xi.M)] < [\mathcal{O}(K.Iter.M.Q)+ \mathcal{O}(K.Iter.\xi.M)]$.

VI. Simulation Results

In this section, we present a performance evaluation of the proposed DDPP architecture and the precoding schemes. To ensure a comprehensive analysis, we compare our work to the state-of-the-art techniques presented in references [25] and [33]. We consider a wideband UM-MIMO-OFDM system with $M = 128$ subcarriers operating at a carrier frequency of $f_c = 300$ GHz and a bandwidth of $B = 30$ GHz. The BS in this system is equipped with a ULA consisting of $N_{\mathrm{T}} = 256$ half-wavelength spaced antennas. The BS also incorporates $K = 16$ TTDs, along with $N_{\mathrm{RF}} = 4$ RF chains. The THz band channel is known for its highly directional propagation, and is commonly referred to as a LoS-dominant channel [40], [41]. As such, we assume that there is only one path per user, i.e., $L = 1$.

As for the hardware constraints, we consider TTDs with a time delay resolution of $t_{\mathrm{res}} = 4$ ps [42]. The proposed DDPP architecture requires a maximum time delay of 26.67 ps for $\theta_{l,u} = \pi/2$, as calculated using (11). Therefore, we limit the TTDs to a maximum delay range of $t_{\max} = 28$ ps, which is an integer multiple of t_{res}. For comparison, we also consider TTDs with a maximum delay range of $t_{\max} = 340$ ps as used in [33]. Besides, we consider low-resolution PSs digitally controlled by $b = 1$and2 bits. We assume $Iter = 5$ and $\epsilon = 10^{-2}$ as the convergence conditions for the proposed HPP.

In terms of evaluation metrics, we consider the normalized array gain per user $g(\theta_{l,u})$, which is defined as the array gain normalized to that achieved by an unconstrained full-TTD precoder averaged over subcarriers for a given user and expressed as

$$g(\theta_{l,u}) = \frac{1}{M} \sum_{m=1}^{M} g_m(\theta_{l,u}). \tag{47}$$

Furthermore, we also consider the normalized array gain per multiple users with random orientations $\theta_{l,u} \in [0, \pi]$, which is given as

$$\bar{g} = \frac{1}{U} \sum_{u=1}^{U} g(\theta_{l,u}). \tag{48}$$

Additionally, we consider the spectral efficiency per subcarrier, which is calculated as

$$R = \frac{1}{M} \sum_{m=1}^{M} \log_2 \left(|\mathbf{I}_U + SNR.\mathbf{H}_{\mathrm{m}} \mathbf{A} \mathbf{X}_m \mathbf{D}_m \mathbf{D}_m^H \mathbf{X}_m^H \mathbf{A}^H \mathbf{H}_{\mathrm{m}}^H| \right), \tag{49}$$

where SNR denotes the signal-to-noise ratio per subcarrier. In order to suppress inter-user inter-

ference, we adopt zero-forcing digital precoding $\mathbf{D}_m = \mathbf{H}_{\text{eff},m}^H(\mathbf{H}_{\text{eff},m}\mathbf{H}_{\text{eff},m}^H)^{-1}$, where $\mathbf{H}_{\text{eff},m} = \mathbf{H}_m\mathbf{A}\mathbf{X}_m$ denotes the effective channel at the m^{th} subcarrier. The digital precoder $\mathbf{D}_m$ is normalized where the total transmit power constraint is met, such that $\|\mathbf{A}\mathbf{X}_m\mathbf{D}_m\|_F^2 = N_{\text{s}}$. Simulation results are averaged over 1000 iterations.

A. Hybrid Analog Precoding under Limited-Range TTD Constraint

In this subsection, we present a performance comparison of the proposed DDPP precoding scheme with the hybrid precoding schemes proposed in [25] and [33] considering practical limited-range TTDs.

Fig.3 presents the normalized array gain per multiple users versus the maxmimum delay range $t_{\max}$. It can be observed that the normalized array gain per multiple users increases as $t_{\max}$ scales up. For $t_{\max} = 10$ ps, the normalized array gain per multiple users of the hybrid precoding in [25] is nearly 0.3, which increases to 0.86 for $t_{\max} = 350$ ps. The hybrid precoding in [33] achieves a slightly higher performance, reaching 0.93 for $t_{\max} = 350$ ps. In contrast, the proposed DDPP achieves a much higher performance of 0.96 for $t_{\max} = 28$ ps. This remarkable improvement is due to the proposed DDPP architecture, which does not require the maximum time delay to scale up with the TTD's index. In particular, the maximum time delay required by the proposed DDPP is Δt_k^n, whereas the hybrid precoding in [25] requires $(K-1)\Delta t_k^n$. When $\theta_{l,u} = \pi/2$, the maximum time delay required by the proposed DDPP is 26.67 ps per (11), whereas a maximum time delay of 400 ps is required by the DPP architecture as calculated by (8).

Fig.4 depicts the normalized array gain per multiple users versus the number of antennas N_{T} for $t_{\max} = 340$ ps and $t_{\max} = 28$ ps. We increase the number of TTDs $K \in \{4,\ 8,\ 16,\ 32,\ 64\}$ as the number of antenna elements increases $N_{\text{T}} = \{64,\ 128,\ 256,\ 512,\ 1024\}$ such that the ratio $Q = N_{\text{T}}/K = 16$ remains constant, thereby ensuring the same level of robustness against beam squint effect. The results show that the normalized array gain per multiple users of the hybrid precodings in [25] and [33] decreases significantly as the number of antennas increases. Specifically, it drops from nearly 0.8 to less than 0.2 for $t_{\max} = 28$ ps, and from 0.96 to less than 0.4 for $t_{\max} = 340$ ps. This degradation is due to the maximum required delay range of [25] and [33], which increases with the number of TTDs. In constrast, the proposed DDPP maintains a normalized array gain per multiple users of 0.96 as the number of antenna elements increases for $t_{\max} = 28$ ps. This is due to the maximum required time delay not scaling with K, making the proposed DDPP scalable and thus suitable for UM-MIMO systems.

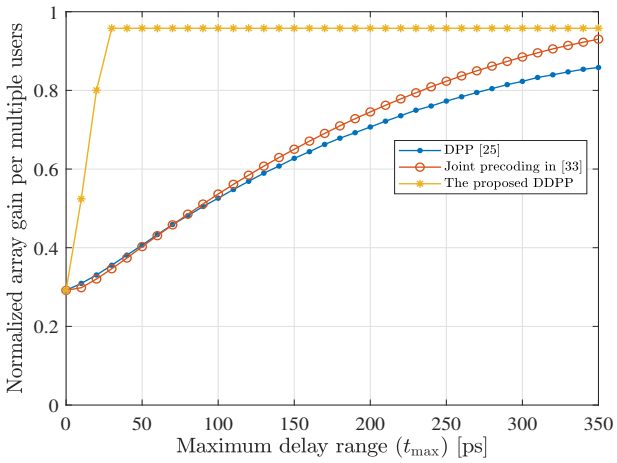

Fig. 3: normalized array gain per multiple users versus maximum delay range $t_{\max}$.

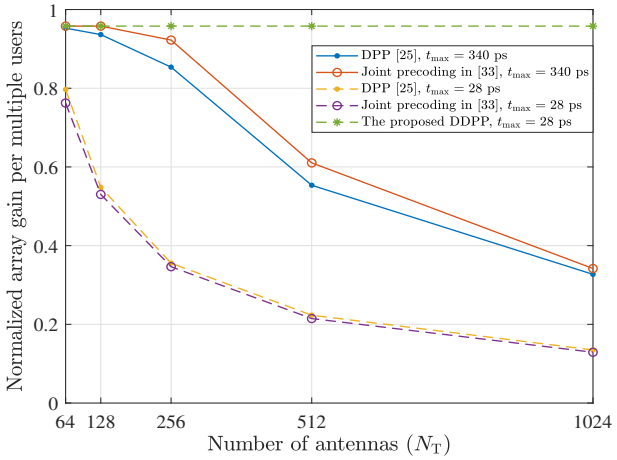

Fig. 4: normalized array gain per multiple users versus number of antennas N_{T} when $t_{\max} = 28$ and 340 ps.

With the aim of investigating the performance of the proposed DDPP precoding scheme deeper, we plot in Fig.5 the normalized array gain over subcarriers for DDPP compared to the hybrid precoding schemes in [25] and [33]. We consider practical limited-range TTDs with $t_{\max} = 28$ ps and $t_{\max} = 340$ ps, where $N_{\mathrm{T}} = 256$, $K = 16$, and $\sin(\theta_{l,u}) = 0.8$. Our investigation reveals that the proposed DDPP exhibits the same degree of robustness against beam squint effect as the hybrid precoding in [33] when $t_{\max} = 340$ ps. Specifically, the normalized array gain of all subcarriers is higher than 0.8 in both approaches. Notably, the proposed DDPP achieves a higher degree of robustness against beam squint effect than DPP approach in [25], where the normalized array gain of [25] drops to lower than 0.8 at margin subcarriers when $t_{\max} = 340$ ps. On the other hand, the normalized array gain of the hybrid precodings in [25] and [33] drops down fluctuating around 0.1 at non-central subcarriers when $t_{\max} = 28$ ps. However, the proposed

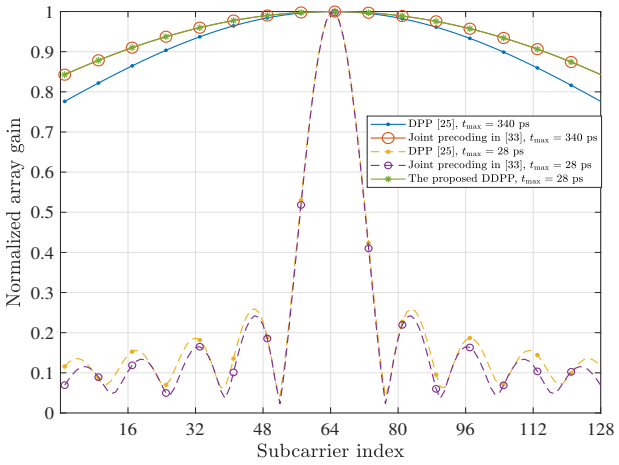

Fig. 5: Normalized array gain versus subcarrier index when $\sin(\theta_{l,u}) = 0.8$ and $t_{\max} = 28$ ps and $t_{\max} = 340$ ps.

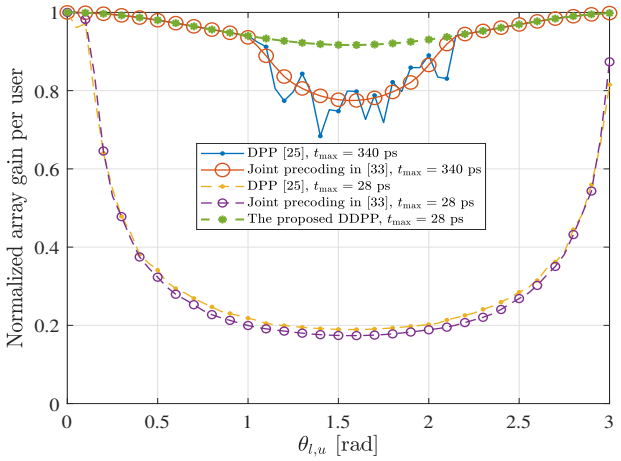

Fig. 6: normalized array gain per user versus $\theta_{l,u}$ when $t_{\max} = 28$ and 340 ps.

DDPP maintains its robustness achieving a normalized array gain over 0.8 for all subcarriers.

To further evaluate the performance of DDPP compared to the reference works, Fig.6 illustrates the normalized array gain per user versus $\theta_{l,u} \in [0, \pi]$ for $t_{\max} = 340$ and 28 ps. It is observed that the normalized array gain per user of the hybrid precodings in [25] and [33] declines as $\theta_{l,u}$ approaches $\pi/2$, where the normalized array gain per user is lower than 0.8 at $\theta_{l,u} = \pi/2$ when $t_{\max} = 340$ ps. Moreover, the normalized array gain per user of the hybrid precodings in [25] and [33] deteriorates to around 0.2 at $\theta_{l,u} = \pi/2$ when $t_{\max} = 28$ ps. This happens because the required time delay scales up as $\sin(\theta_{l,u})$ approaches 1 as shown in (11). Meanwhile, the proposed DDPP maintains a high degree of robustness against beam squint effect, where the normalized array gain per user is higher than 0.9 is guaranteed at all angles when $t_{\max} = 28$ ps.

This superior performance is attributed to the proposed DDPP architecture, which reduces the maximum required delay range by a factor of $K - 1$.

B. Hybrid Analog Precoding under Limited-Range and Finite-Resolution TTD Constraints

In this subsection, we evaluate the peformance of the proposed TR-HP compared to the works in [25] and [33] when considering TTDs with limited-range and finite-resolution. Our main focus is to demonstrate the impact of time delay resolution, thus we consider practical TTDs with $t_{\max} = 340$ ps and $t_{\text{res}} = 4$ ps.

Fig.7 illustrates the impact of time delay resolution on the normalized array gain over subcarriers for $t_{\max} = 340$ ps, $t_{\text{res}} = 4$ ps, and $\sin(\theta_{l,u}) = 0.8$. The results show that the precoding schems in [25] and [33] suffer from a severe performance degradation due to the time delay resolution of TTDs, where the normalized array gain drops below 0.1 and 0.3 for all subcarriers, respectively. On the other hand, the proposed TR-HP achieves a normalized array gain higher than 0.8 at all subcarriers.

Fig.8 shows the normalized array gain per user versus $\theta_{l,u}$ for TTDs with $t_{\max} = 340$ ps and $t_{\text{res}} = 4$ ps. It can be noted that the normalized array gain per user of the hybrid precoding in [25] drops below 0.1 at several angles, while the normalized array gain per user of the hybrid precoding in [33] fluctuates and declines to less than 0.2 at various angles. Nevertheless, the proposed TR-HP achieve normalized array gain very similar to that of the unconstrained DDPP precoder, with a normalized array gain per user greater than 0.9 at all angles.

Fig.9 shows the spectral efficiency performance for $U = N_{\text{s}} = 4$, $t_{\max} = 340$ ps and $t_{\text{res}} = 4$ ps. It can be observed that the proposed TR-HP achieves a spectral efficiency of almost 97% of that achieved by the full-digital precoder, despite the limited-range and finite-resolution constraints of TTDs. Specifically, the spectral efficiency of the proposed TR-HP is almost 21 bps/Hz higher

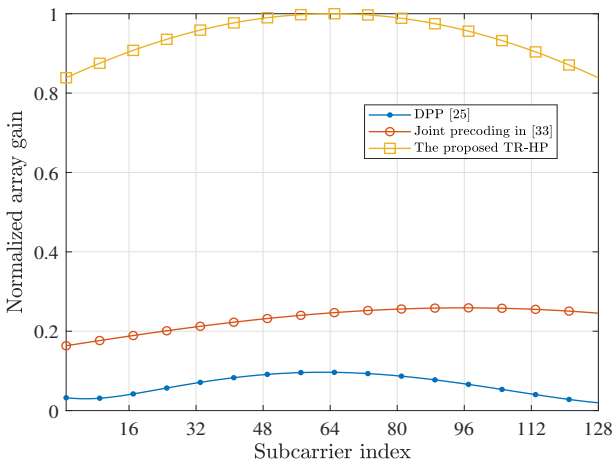

Fig. 7: Normalized array gain versus subcarrier index when $t_{\text{res}} = 4$ ps and $\sin(\theta_{l,u}) = 0.8$.

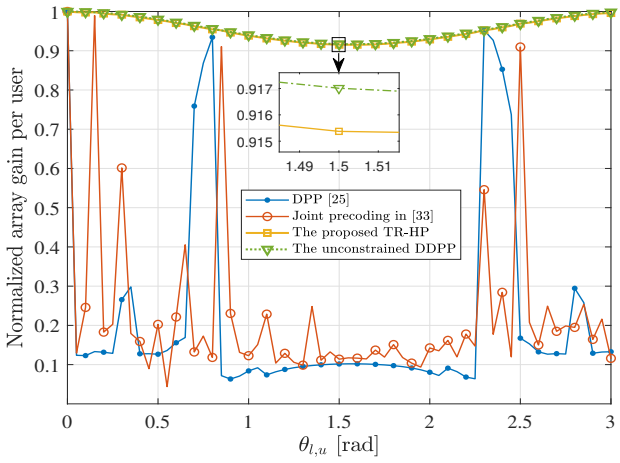

Fig. 8: normalized array gain per user versus $\theta_{l,u}$ when $t_{\max} = 340$ ps and $t_{\text{res}} = 4$ ps.

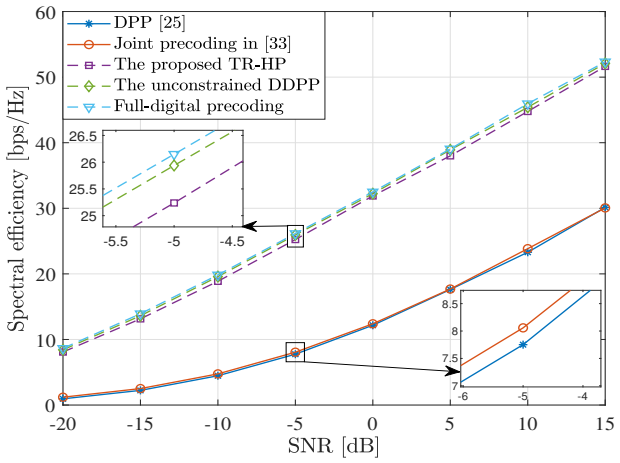

Fig. 9: Spectral efficiency versus SNR when $t_{\max} = 340$ ps and $t_{\text{res}} = 4$ ps.

than that achieved by the hybrid precodings in [25] and [33] at $SNR = 10$ dB.

We conclude that the proposed TR-HP achieves angle-independent performance close to optimal under the hardware constraints of TTDs.

C. Hybrid Precoding with Practical TTD and PS Constraints

In this subsection, we evaluate the performance of the proposed HPP under the consideration of the resolution constraint of PSs in addition to the TTDs constraints considered in the previous subsection. Particularly, we adopt low-resolution PSs that are digitally controlled by $b = 2$ bits, as well as limited-range and finite-resolution TTDs with $t_{\max} = 340$ ps and $t_{\text{res}} = 4$ ps.

Fig.10 illustrates the normalized array gain over subcarriers, considering limited-range and finite-resolution TTDs with $t_{\max} = 340$ ps, $t_{\text{res}} = 4$ ps and low-resolution PSs controlled by $b = 2$ bits, with $\sin(\theta_{l,u}) = 0.8$. The results show that the hybrid precoding in [33] achieves a

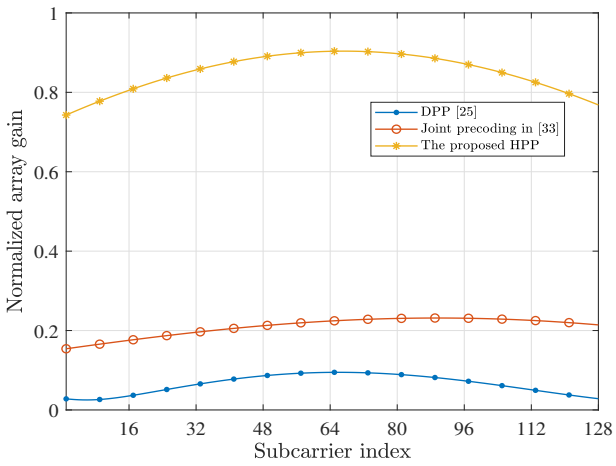

Fig. 10: normalized array gain per user versus subcarrier index when $t_{\max} = 340$ ps, $t_{\text{res}} = 4$ ps, $b = 2$ bits, and $\sin(\theta_{l,u}) = 0.8$.

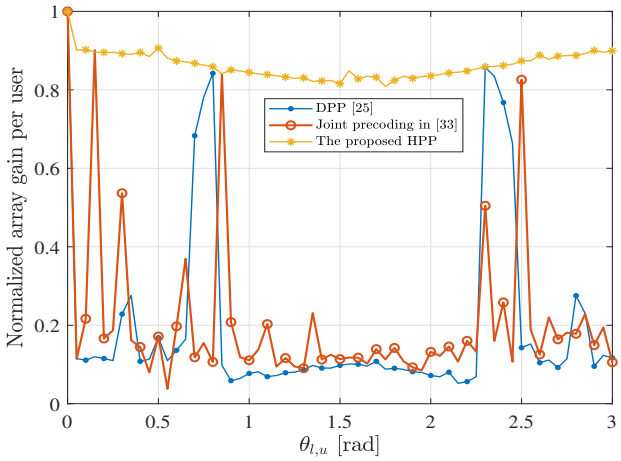

Fig. 11: normalized array gain per user versus $\theta_{l,u}$ when $t_{\max} = 340$ ps, $t_{\text{res}} = 4$ ps, $b = 2$ bits, and $\sin(\theta_{l,u}) = 0.8$.

normalized array gain of around 0.2, while the hybrid precoding in [25] falls below 0.1 at all subcarriers. In contrast, the proposed HPP maintains a normalized array gain higher than 0.7 at all subcarriers.

Similar to Fig.8, Fig.11 depicts the normalized array gain per user versus $\theta_{l,u}$ for $t_{\max} = 340$ ps, $t_{\text{res}} = 4$ ps, and $b = 2$ bits. The hybrid precodings in [25] and [33] exhibit a low normalized array gain per user of 0.1 at several angles. Meanwhile, the proposed HPP achieves a normalized array gain higher than 0.8 at all subcarriers, despite the hardware limitations of TTDs and PSs.

As the iterations represent the penalty of iterative methods, it is meaningful to study the effect of iteration number on the achieved performance. Fig.12 depicts $\bar{g}/\bar{g}_{Iter}$ versus iteration number for different number of antennas, where $\bar{g}_{Iter}$ is the normalized array gain per multiple users at the last iteration. We assume $Iter = 10$, $t_{\max} = 28$ ps, $t_{\text{res}} = 4$ ps and $b = 2$ bits. It is observed

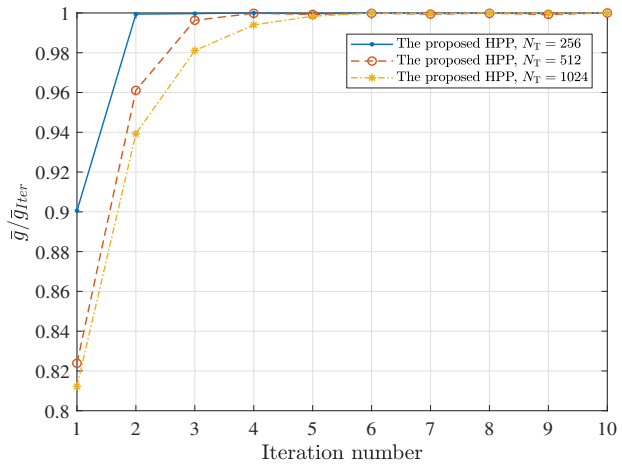

Fig. 12: normalized array gain per multiple users versus iteration number when $t_{\max} = 28$ ps, $t_{\mathrm{res}} = 4$ ps and $b = 2$ bits.

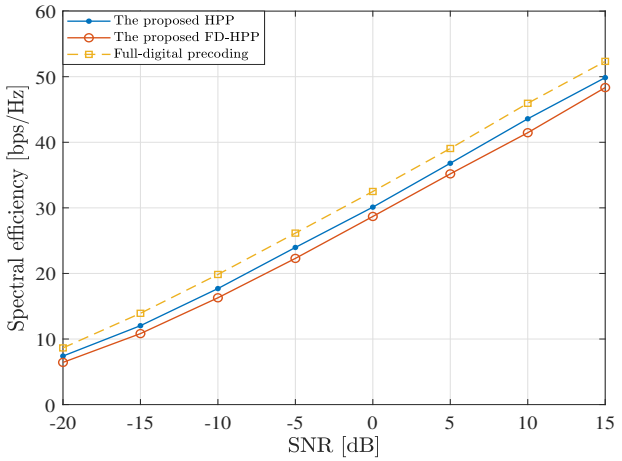

Fig. 13: Spectral efficiency versus SNR when $t_{\max} = 28$ ps, $t_{\mathrm{res}} = 4$ ps, and $b = 2$ bits.

that the proposed HPP has a fast convergence, where $\bar{g}/\bar{g}_{Iter} \geq 0.99$ is reached in 2, 4, and 5 iterations for $N_{\mathrm{T}} = 256,\ 512,$ and 1024, respectively. This confirms the fast convergence and scalability of the proposed HPP, despite the hardware constraints of TTDs and PSs.

Fig.13 depicts the spectral efficiency of the proposed HPP and FD-HPP precoding schemes assuming $U = N_{\mathrm{s}} = 4$, $t_{\max} = 28$ ps, $t_{\mathrm{res}} = 4$ ps, and $b = 2$ bits. It is observed that the spectral efficiency is only 2 bps/Hz lower than that that achieved by the full-digital precoder at $SNR = 10$ dB. We conclude that the proposed HPP achieves near-optimal performance under the adoption of practical TTDs and PSs.

Similarly, the proposed FD-HPP achieves lower computational complexity at the cost of a slight performance reduction. Particularly, the spectral efficiency decreases by only 2 bps/Hz compared to HPP at $SNR = 10$ dB. In concise, the proposed FD-HPP proves to achieve a satisfactory performance with low computational overhead while adhering to the harware

limitations of TTDs and PSs.

VII. CONCLUSION

In this work, we propose a novel hybrid precoding architecture along with several hardware-aware delay-phase precoding schemes that address the beam squint effect while complying with the hardware limitations of TTDs and PSs. The proposed DDPP architecture significantly mitigates the burden of the maximum delay range constraint imposed on TTDs, where the required maximum delay range is reduced by a factor of $(K-1)$ compared to the traditional DPP architecture. Subsequently, we propose TR-HP that additionally addresses the time resolution constraint of TTDs. Specifically, we convert the time error resulting from the finite-resolution constraint of TTDs to the phase domain, where we compensate by introducing an equalization phase shift. Afterwards, we include the resolution constraint of PSs, where we propose HPP scheme that jointly optimizes TTDs and PSs under the consideration of their hardware limitations. In specific, we formulate the design of the hybrid analog precoder under TTDs and PSs constraints as a mixed-integer optimization problem and propose an alternating minimization-based iterative algorithm to solve this problem. Eventually, with the aim of reducing the computational complexity of HPP, we propose FD-HPP, which ensures a fixed time delay value for all TTDs while maintaining lower computational overhead compared to HPP. Simulation results validate the effectiveness of the proposed hybrid precoding schemes under the adoption of the DDPP architecture that utilizes practical TTDs and PSs.

REFERENCES

[1] A. Najjar, M. El-Absi, and T. Kaiser, "Joint Iterative Delay-Phase Precoding for THz UM-MIMO with Finite-Resolution and Limited-Range True Time Delay," in *ICC 2023 - IEEE International Conference on Communications*, 2023. Accepted for publication.

[2] "The Next Hyper Connected Experience for All," White Paper, Samsung 6G Vision, June. 2020.

[3] W. Saad, M. Bennis, and M. Chen, "A Vision of 6G Wireless Systems: Applications, Trends, Technologies, and Open Research Problems," *IEEE Network*, vol. 34, no. 3, pp. 134–142, 2020.

[4] F. Hu, Y. Deng, W. Saad, M. Bennis, and A. H. Aghvami, "Cellular-Connected Wireless Virtual Reality: Requirements, Challenges, and Solutions," *IEEE Communications Magazine*, vol. 58, no. 5, pp. 105–111, 2020.

[5] Z. Chen, C. Han, Y. Wu, L. Li, C. Huang, Z. Zhang, G. Wang, and W. Tong, "Terahertz Wireless Communications for 2030 and Beyond: A Cutting-Edge Frontier," *IEEE Communications Magazine*, vol. 59, no. 11, pp. 66–72, 2021.

[6] J. C. Balzer, C. J. Saraceno, M. Koch, P. Kaurav, U. R. Pfeiffer, W. Withayachumnankul, T. Kürner, A. Stöhr, M. El-Absi, A. A.-H. Abbas, T. Kaiser, and A. Czylwik, "THz Systems Exploiting Photonics and Communications Technologies," *IEEE Journal of Microwaves*, vol. 3, no. 1, pp. 268–288, 2023.

[7] M. El-Absi, A. Alhaj Abbas, A. Abuelhaija, F. Zheng, K. Solbach, and T. Kaiser, "High-Accuracy Indoor Localization Based on Chipless RFID Systems at THz Band," *IEEE Access*, vol. 6, pp. 54355–54368, 2018.

[8] J. Kokkoniemi, J. Lehtomäki, and M. Juntti, "A Discussion on Molecular Absorption Noise in the Terahertz Band," *Nano Communication Networks*, vol. 8, pp. 35–45, 2016. Electromagnetic Communication in Nano-scale.

[9] I. F. Akyildiz, C. Han, and S. Nie, "Combating the Distance Problem in the Millimeter wave and Terahertz Frequency Bands," *IEEE Communications Magazine*, vol. 56, no. 6, pp. 102–108, 2018.

[10] H. Sarieddeen, M.-S. Alouini, and T. Y. Al-Naffouri, "Terahertz-Band Ultra-Massive Spatial Modulation MIMO," *IEEE Journal on Selected Areas in Communications*, vol. 37, no. 9, pp. 2040–2052, 2019.

[11] M. R. Akdeniz, Y. Liu, M. K. Samimi, S. Sun, S. Rangan, T. S. Rappaport, and E. Erkip, "Millimeter wave Channel Modeling and Cellular Capacity Evaluation," *IEEE Journal on Selected Areas in Communications*, vol. 32, no. 6, pp. 1164–1179, 2014.

[12] C. Han, A. O. Bicen, and I. F. Akyildiz, "Multi-Wideband Waveform Design for Distance-Adaptive Wireless Communications in the Terahertz Band," *IEEE Transactions on Signal Processing*, vol. 64, no. 4, pp. 910–922, 2016.

[13] I. F. Akyildiz and J. M. Jornet, "Realizing Ultra-Massive MIMO (1024×1024) Communication in the (0.06–10) Terahertz Band," *Nano Communication Networks*, vol. 8, pp. 46–54, 2016. Electromagnetic Communication in Nano-scale.

[14] W. Roh, J.-Y. Seol, J. Park, B. Lee, J. Lee, Y. Kim, J. Cho, K. Cheun, and F. Aryanfar, "Millimeter-wave Beamforming as an Enabling Technology for 5G Cellular Communications: Theoretical Feasibility and Prototype Results," *IEEE Communications Magazine*, vol. 52, pp. 106–113, 2014.

[15] D. Ha, K. Lee, and J. Kang, "Energy Efficiency Analysis with Circuit Power Consumption in Massive MIMO Systems," in *2013 IEEE 24th Annual International Symposium on Personal, Indoor, and Mobile Radio Communications (PIMRC)*, pp. 938–942, 2013.

[16] S. Han, C.-l. I, Z. Xu, and C. Rowell, "Large-Scale Antenna Systems with Hybrid Analog and Digital Beamforming for Millimeter wave 5G," *IEEE Communications Magazine*, vol. 53, no. 1, pp. 186–194, 2015.

[17] A. Najjar, M. El-Absi, and T. Kaiser, "Dynamic Array of Subarrays Architecture based Hybrid Beamforming in UM-MIMO Systems," in *2021 Fourth International Workshop on Mobile Terahertz Systems (IWMTS)*, pp. 1–5, 2021.

[18] C. Han, L. Yan, and J. Yuan, "Hybrid Beamforming for Terahertz Wireless Communications: Challenges, Architectures, and Open Problems," *IEEE Wireless Communications*, vol. 28, no. 4, pp. 198–204, 2021.

[19] Y. Chen and C. Han, "Razor-Sharp Narrowbeam Communications and Management for Terahertz Wireless Networks (Invited Paper)," in *2021 Computing, Communications and IoT Applications (ComComAp)*, pp. 335–340, 2021.

[20] H. Hashemi, T.-s. Chu, and J. Roderick, "Integrated True-Time-Delay-based Ultra-Wideband Array Processing," *IEEE Communications Magazine*, vol. 46, no. 9, pp. 162–172, 2008.

[21] C. Lin, G. Li, and L. Wang, "Subarray-based Coordinated Beamforming Training for mmwave and Sub-THz Communications," *IEEE Journal on Selected Areas in Communications*, vol. PP, pp. 1–1, 06 2017.

[22] S. A. Busari, K. M. S. Huq, S. Mumtaz, J. Rodriguez, Y. Fang, D. C. Sicker, S. Al-Rubaye, and A. Tsourdos, "Generalized Hybrid Beamforming for Vehicular Connectivity Using THz Massive MIMO," *IEEE Transactions on Vehicular Technology*, vol. 68, no. 9, pp. 8372–8383, 2019.

[23] J. Tan and L. Dai, "THz Precoding for 6G: Challenges, Solutions, and Opportunities," *IEEE Wireless Communications*, pp. 1–8, 2022.

[24] J. Tan and L. Dai, "Delay-Phase Precoding for THz Massive MIMO with Beam Split," in *2019 IEEE Global Communications Conference (GLOBECOM)*, pp. 1–6, 2019.

[25] L. Dai, J. Tan, Z. Chen, and H. V. Poor, "Delay-Phase Precoding for Wideband THz Massive MIMO," *IEEE Transactions on Wireless Communications*, vol. 21, no. 9, pp. 7271–7286, 2022.

[26] Y. Wu, G. Song, H. Liu, L. Xiao, and T. Jiang, "3-D Hybrid Beamforming for Terahertz Broadband Communication System with Beam Squint," *IEEE Transactions on Broadcasting*, pp. 1–12, 2022.

[27] D. Baltimas and G. M. Rebeiz, "A 25–50 GHz Phase Change Material (PCM) 5-bit True Time Delay Phase Shifter in a Production SiGe BiCMOS Process," in *2021 IEEE MTT-S International Microwave Symposium (IMS)*, pp. 435–437, 2021.

[28] A. Karakuzulu, M. H. Eissa, D. Kissinger, and A. Malignaggi, "Broadband 110 - 170 GHz True Time Delay Circuit in a 130-nm SiGE BiCMOS Technology," in *2020 IEEE/MTT-S International Microwave Symposium (IMS)*, pp. 775–778, 2020.

[29] J. Shen, Y. Zhang, L. Yang, L. He, Y. Guo, and H. Gao, "Wideband Digitally Controlled True Time Delay for Beamforming in a 40 nm CMOS Technology," in *2021 IEEE International Symposium on Circuits and Systems (ISCAS)*, pp. 1–4, 2021.

[30] P. Raviteja, Y. Hong, and E. Viterbo, "Analog Beamforming with Low Resolution Phase Shifters," *IEEE Wireless Communications Letters*, vol. 6, no. 4, pp. 502–505, 2017.

[31] L. Yan, C. Han, and J. Yuan, "Energy-Efficient Dynamic-Subarray with Fixed True-Time-Delay Design for Terahertz Wideband Hybrid Beamforming," *IEEE Journal on Selected Areas in Communications*, vol. 40, no. 10, pp. 2840–2854, 2022.

[32] D. Q. Nguyen and T. Kim, "Joint Delay and Phase Precoding under True-Time Delay Constraints for THz Massive MIMO," in *ICC 2022 - IEEE International Conference on Communications*, pp. 3496–3501, 2022.

[33] D. Q. Nguyen and T. Kim, "True-Time Delay-Based Hybrid Precoding Under Time Delay Constraints in Wideband THz Massive MIMO Systems," Dec. 2022. *arXiv:2212.07484v3 [eess.SP]*.

[34] E. Ghaderi, A. Sivadhasan Ramani, A. A. Rahimi, D. Heo, S. Shekhar, and S. Gupta, "An Integrated Discrete-Time Delay-Compensating Technique for Large-Array Beamformers," *IEEE Transactions on Circuits and Systems I: Regular Papers*, vol. 66, no. 9, pp. 3296–3306, 2019.

[35] B. Zhai, Y. Zhu, A. Tang, and X. Wang, "THzPrism: Frequency-based Beam Spreading for Terahertz Communication Systems," *IEEE Wireless Communications Letters*, vol. 9, no. 6, pp. 897–900, 2020.

[36] A. Najjar, M. El-Absi, and T. Kaiser, "Non-Overlapped Subarrays based Wideband Delay-Phase Hybrid Beamforming," in *2022 Fifth International Workshop on Mobile Terahertz Systems (IWMTS)*, pp. 1–5, 2022.

[37] L. Yan, C. Han, T. Yang, and J. Yuan, "Dynamic-subarray with Fixed-True-Time-Delay Architecture for Terahertz Wideband Hybrid Beamforming," in *2021 IEEE Global Communications Conference (GLOBECOM)*, pp. 1–6, 2021.

[38] S. Boyd and L. Vandenberghe, *Convex Optimization*. Cambridge University Press, 2004.

[39] J. W. Brown and R. V. Churchill, *Complex Variables and Applications*. Boston, MA: McGraw-Hill Higher Education, eighth ed., 2009.

[40] O. E. Ayach, S. Rajagopal, S. Abu-Surra, Z. Pi, and R. W. Heath, "Spatially Sparse Precoding in Millimeter wave MIMO Systems," *IEEE Transactions on Wireless Communications*, vol. 13, no. 3, pp. 1499–1513, 2014.

[41] T. S. Rappaport, G. R. MacCartney, M. K. Samimi, and S. Sun, "Wideband Millimeter-wave Propagation Measurements and Channel Models for Future Wireless Communication System Design," *IEEE Transactions on Communications*, vol. 63, no. 9, pp. 3029–3056, 2015.

[42] M.-K. Cho, I. Song, and J. D. Cressler, "A True Time Delay-based SiGe Bi-directional T/R Chipset for Large-Scale Wideband Timed Array Antennas," in *2018 IEEE Radio Frequency Integrated Circuits Symposium (RFIC)*, pp. 272–275, 2018.